Image-domain Full Waveform Inversion: field data example

Sanzong Zhang and Gerard Schuster, King Abdullah University of Science and Technology

SUMMARY

The main difficulty with the data-domain full waveform inversion (FWI) is that it tends to get stuck in the local minima associated with the waveform misfit function. This is the result of cycle skipping which degrades the low-wavenumber update in the absence of low-frequencies and long-offset data. An image-domain objective function is defined as the normed difference between the predicted and observed common image gathers (CIGs) in the subsurface offset domain. This new objective function is not constrained by cycle skipping at the far subsurface offsets. To test the effectiveness of this method, we apply it to marine data recorded in the Gulf of Mexico. Results show that image-domain FWI is less sensitive to the initial model and the absence of low-frequency data compared with conventional FWI. The liability, however, is that it is almost an order of magnitude more expensive than standard FWI.

INTRODUCTION

An accurate velocity model is a prerequisite for accurately imaging complex geological structures. To improve the resolution of the velocity model, wave-equation tomography is proposed to invert the waveform information for fine details of the earth model. This procedure can be divided into two categories. The first category defines the objective function in the data domain to best fit the traveltime or waveform information in the observed data. The second category defines an objective function in the image domain to flatten the angle-domain, offset-domain or shot-domain CIGs, or focus the subsurface-offset-domain CIGs.

FWI is a data-domain wave-equation inversion method. The problem with FWI is that its objective function can be highly nonlinear with respect to velocity perturbations, so that it tends to get stuck in local minima. This results in cycle skipping if the velocity model is far from the true velocity model. To reduce the nonlinearity, FWI requires the low-frequency or long-offset components in the observed data. DSO (Symes and Kern, 1994; Yang et al., 2013) uses the first derivative of the migration image along the angle axis to produce the image perturbation. It also uses the subsurface-offset-domain data to construct a penalty operator, which annihilates the energy at nonzero lags, and enhances the migration energy at zero lag.

Zhang and Schuster (2013) proposed a new image-domain wave-equation inversion method, which minimizes the difference of the subsurface-offset-domain image obtained by migrating the waveform residual in the data-domain. The gradient of this objective function is composed of two parts. One part demigrates the subsurface-offset-domain image residual to get the predicted data residual and reverse-time migrate it. This term is the scaled gradient of the conventional FWI and is used to update the high-wavenumber components of velocity. The second part smears the data residual along subsurface-offset-domain wavepath to update the velocity model. This term does not suffer from the cycle skipping problem like DSO and is used to update the low-wavenumbers components of velocity. Now we present tests of this method on marine data recorded in the Gulf of Mexico.

THEORY

The cross-correlation between the forward wavefield $p_s(\mathbf{x},\omega|\mathbf{x}_s)$ and the backward wavefield $p_g(\mathbf{x},\omega|\mathbf{x}_s)$ can be used to determine the subsurface-offset-domain image

$$m(\mathbf{x},\mathbf{h}) = \sum_{\mathbf{x}_s,\mathbf{x}_g,\omega} p_s(\mathbf{x}-\mathbf{h},\omega|\mathbf{x}_s)\, p_g^*(\mathbf{x}+\mathbf{h},\omega|\mathbf{x}_s), \qquad (1)$$

where $p_s(\mathbf{x}-\mathbf{h},\omega|\mathbf{x}_s)$ is the forward modeled wavefield at the subsurface offset location $\mathbf{x}$ initiated by the source wavelet $W(\omega)$ at the location $\mathbf{x}_s$,

$$p_s(\mathbf{x},\omega|\mathbf{x}_s) = W(\omega)G(\mathbf{x},\omega|\mathbf{x}_s), \qquad (2)$$

and $p_g(\mathbf{x},\omega|\mathbf{x}_s)$ is the backpropagated reflection field at $\mathbf{x}$ from the observed data $p(\mathbf{x}_g,t|\mathbf{x}_s)_{obs}$ recorded by the geophones located at $\mathbf{x}_g$,

$$p_g(\mathbf{x},\omega|\mathbf{x}_s) = \sum_{\mathbf{x}_g} d(\mathbf{x}_g,\omega|\mathbf{x}_s)G^*(\mathbf{x},\omega|\mathbf{x}_g), \qquad (3)$$

where $\mathbf{h}$ is the space-lag in the cross-correlation function in equation 1, and also can be denoted as the subsurface-offset. The start symbol * represents convolution with respect to time, and $g(\mathbf{x},\omega|\mathbf{x}_s)$ is the Green's function. We assume a standard migration method that migrates shot gathers recorded on the surface to give the function $m(\mathbf{x},\mathbf{h})$, abbreviated as the subsurface-offset domain image at the subsurface offset position. For $h=0$, $m(\mathbf{x},0)$ reduces to the conventional migration image.

By substituting equation 2 and equation 3 into equation 1, we can obtain

$$m(\mathbf{x},\mathbf{h}) = \sum_{\mathbf{x}_s,\mathbf{x}_g,\omega} W(\omega)G(\mathbf{x}-\mathbf{h},\omega|\mathbf{x}_s) \\ G(\mathbf{x}+\mathbf{h},\omega|\mathbf{x}_g)d(\mathbf{x}_g,\omega|\mathbf{x}_s)^*. \qquad (4)$$

The inverse problem is defined as finding a velocity model that minimizes the following misfit function,

$$\varepsilon = \frac{1}{2}\sum_{\mathbf{x},\mathbf{h}} [m(\mathbf{x},\mathbf{h})_{cal} - m(\mathbf{x},\mathbf{h})_{obs}]^2, \qquad (5)$$

where $m(\mathbf{x},\mathbf{h})_{cal}$ and $m(\mathbf{x},\mathbf{h})_{obs}$ are the subsurface-offset-domain images obtained by migrating the modeled data and the observed data, respectively. The optimal estimate of velocity

DOI http://dx.doi.org/10.1190/segam2014-1441.1

model minimizes the image intensity of the nonzero subsurface-offset gathers and focuses the image at the zero subsurface-offset. $m(\mathbf{x},\mathbf{h})_{obs}$ spreads the image energy at nonzero lags if there are errors in the velocity model. Since the forward modeling and migration use the same velocity model, $m(\mathbf{x},\mathbf{h})_{cal}$ is always a focused image. The exception is that $m(\mathbf{x},\mathbf{h})_{cal}$ not only focus at zero subsurface-offset, but spreads some image energy along the non-zero subsurface-offset in the complex region with poor illumination. This phenomenon violates the criterion of DSO. Compared with DSO, image-domain FWI removes these effects by subtracting the background focused image associated with the modeled data from the unfocused image associated with the observed data.

The gradient of the misfit function is written as

$$g(\mathbf{x}') = \sum_{\mathbf{x},\mathbf{h}} \Delta m(\mathbf{x},\mathbf{h}) \frac{\partial \Delta m(\mathbf{x},\mathbf{h})}{\partial c(\mathbf{x}')}, \tag{6}$$

where the image residual is defined as

$$\Delta m(\mathbf{x},\mathbf{h}) = \sum_{\mathbf{x}_s,\mathbf{x}_g,\omega} W(\omega) G(\mathbf{x}-\mathbf{h},\omega|\mathbf{x}_s) \\ G(\mathbf{x}+\mathbf{h},\omega|\mathbf{x}_g) \Delta d(\mathbf{x}_g,\omega|\mathbf{x}_s)^* \tag{7}$$

and the data residual is computed by

$$\Delta d(\mathbf{x}_g,\omega|\mathbf{x}_s) = d(\mathbf{x}_g,\omega|\mathbf{x}_s)_{cal} - d(\mathbf{x}_g,\omega|\mathbf{x}_s)_{obs}. \tag{8}$$

Under the Born approximation, we have

$$g_1(\mathbf{x}') = -\frac{2}{c(\mathbf{x}')^3} \sum_{\mathbf{x},\mathbf{h},\mathbf{x}_s,\mathbf{x}_g,\omega} \omega^2 W(\omega) G(\mathbf{x}',\omega|\mathbf{x}_s) \\ G(\mathbf{x}-\mathbf{h},\omega|\mathbf{x}') \Delta m(\mathbf{x},\mathbf{h}) G(\mathbf{x}+\mathbf{h},\omega|\mathbf{x}_g) \Delta d(\mathbf{x}_g,\omega|\mathbf{x}_s)^*, \tag{9}$$

$$g_2(\mathbf{x}') = -\frac{2}{c(\mathbf{x}')^3} \sum_{\mathbf{x},\mathbf{h},\mathbf{x}_s,\mathbf{x}_g,\omega} \omega^2 W(\omega) G(\mathbf{x}-\mathbf{h},\omega|\mathbf{x}_s) \\ \Delta m(\mathbf{x},\mathbf{h}) G(\mathbf{x}+\mathbf{h},\omega|\mathbf{x}') G(\mathbf{x}',\omega|\mathbf{x}_g) \Delta d(\mathbf{x}_g,\omega|\mathbf{x}_s)^*, \tag{10}$$

and

$$g_3(\mathbf{x}') = -\frac{2}{c(\mathbf{x}')^3} \sum_{\mathbf{x},\mathbf{h},\mathbf{x}_s,\mathbf{x}_g,\omega} \omega^2 |W(\omega)|^2 G(\mathbf{x}-\mathbf{h},\omega|\mathbf{x}_s) \\ \Delta m(\mathbf{x},\mathbf{h}) G(\mathbf{x}+\mathbf{h},\omega|\mathbf{x}_g) G^*(\mathbf{x}',\omega|\mathbf{x}_s) G^*(\mathbf{x}_g,\omega|\mathbf{x}'). \tag{11}$$

The first term $g_1(\mathbf{x}')$ says that the velocity is updated by weighting the backward propagated data $G^*(\mathbf{x}+\mathbf{h},\omega|\mathbf{x}_g)\Delta d$ with the weighted image residual $\Delta m(\mathbf{x},\mathbf{h})$, and smearing it along the source wavepath from $\mathbf{x_s}$ to $\mathbf{x}-\mathbf{h}$. The second term $g_2(\mathbf{x}')$ is similar, except the velocity is updated by weighting the forward propagated source field $W(\omega)G(\mathbf{x}-\mathbf{h},\omega|\mathbf{x}_s)$ with the image residual $\Delta m(\mathbf{x},\mathbf{h})$, and smearing it along the geophone wavepath from $\mathbf{x_g}$ to $\mathbf{x}-\mathbf{h}$. The sum of the first two terms $g_1(\mathbf{x}')+g_2(\mathbf{x}')$ is equivalent to smearing the data residual along the subsurface-offset-domain wavepath to update the velocity model. The third term is interpreted as calculating the data residual by demigrating the subsurface-offset-domain image-residual $W(\omega)G(\mathbf{x}-\mathbf{h},\omega|\mathbf{x}_s)\Delta m(\mathbf{x},\mathbf{h})G(\mathbf{x}+\mathbf{h},\omega|\mathbf{x}_g)$ and then reverse time migrate the data residual. This term is actually the scaled gradient of the data-domain FWI. The first two terms are similar to the gradient of DSO which updates the low wavenumber components of velocity, and the third term is the gradient of data-domain FWI which updates the high-wavenumber components of velocity.

NUMERICAL EXAMPLES

The numerical example is a real marine data test from the Gulf of Mexico with image-domain FWI. This streamer data set is acquired using 496 shots with a shot interval of 37.5 m, a time-sampling interval of 1 ms, a trace length of 5 s, and 480 active hydrophones per shot. The hydrophone interval is 6.25 m, with a near offset of 198 m and a far offset 6 km, and the source wavelet is estimated by stacking along the first arrival at the nearest offset of each shot. The data are low-passed filtered to the frequency range 0-45 Hz. Actually the frequency below 5 Hz is missing from the data. The initial velocity model is obtained from first-arrival traveltime tomography to give the tomogram in Figure 1. This velocity model is the initial velocity for image-domain FWI, where the turning wave could not penetrate deeper than 2.5 km. We will invert the reflection waves to improve the velocity in the deeper part of the initial velocity model.

The inverted velocity model is displayed in Figure 2. To further verify that the reconstructed velocity model is more accurate than the initial velocity model, we compare the migration images from different velocity models. The RTM image using the velocity model from traveltime tomogram and image-domain FWI are displayed in Figures 3 and 4. Using the inverted velocity model from image-domain FWI, the resulting migration image appears be better focused than that from the traveltime tomography. The angle-domain CIGs calculated from the initial model and inverted model are shown in Figures 5-6, and we can see that the inverted model flattens the angle-domain CIGS better than the initial velocity model in the deeper part. The zoomed views of the migration images are shown in Figures 7(a)-7(d) for a detailed comparison. It is obvious that the image-domain FWI images are better focused than those obtained by traveltime tomography.

Figures 8-11 show the gradients computed by the image-domain FWI and conventional FWI. Figure 8 depicts DSO gradient from image-domain FWI, and Figure 9 is the FWI gradient from image-domain FWI. The sum of the DSO gradients and the FWI gradient is shown in Figure 10. The gradient from conventional FWI is plotted in Figure 11. These figures illustrates that the gradient of image-domain FWI contains more low-wavenumber components than the gradient of the conventional FWI.

DOI http://dx.doi.org/10.1190/segam2014-1441.1

CONCLUSIONS

We present an image-domain FWI method that defines the objective function as the subsurface-offset-domain image residual for the observed data and the calculated data. The image-domain FWI gradient is a combination of the gradients for conventional FWI and DSO. Compared to conventional FWI, image-domain FWI is less sensitive to the initial velocity model and cycle skipping, and is more efficient in updating the low-wavenumber components of velocity. It can also reduce edge effect artifacts and the problem of falsely over-penalized focused images that are inherent in DSO. Numerical examples demonstrate that for the GOM data, image-domain FWI provides a more accurate velocity model than conventional FWI and the initial velocity model is far from the true model. The main limitation of our method is that it requires significantly more computation and memory than FWI.

ACKNOWLEDGMENTS

We thank the 2011 sponsors of Center for Subsurface Imaging and Fluid Modeling (CSIM) at KAUST for their support (www.csim.kaust.edu.sa).

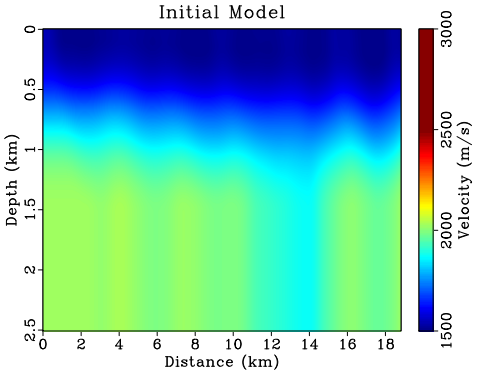

Figure 1: The initial velocity mode.

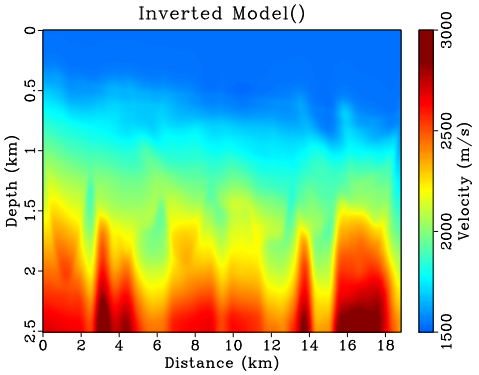

Figure 2: The inverted model after 70 iterations using image-domain FWI.

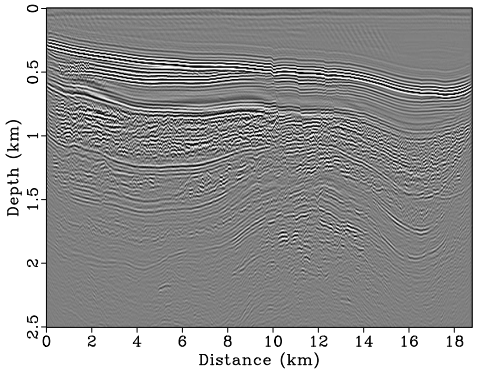

Figure 3: RTM image using the initial velocity model.

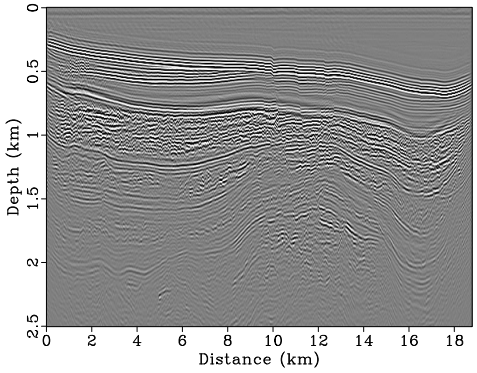

Figure 4: RTM image using the inverted velocity model.

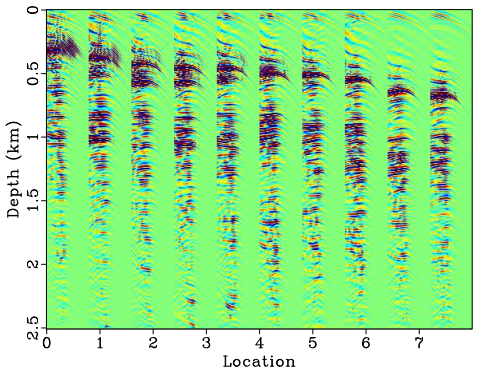

Figure 5: Angle-domain CIGs using the initial velocity model.

DOI http://dx.doi.org/10.1190/segam2014-1441.1

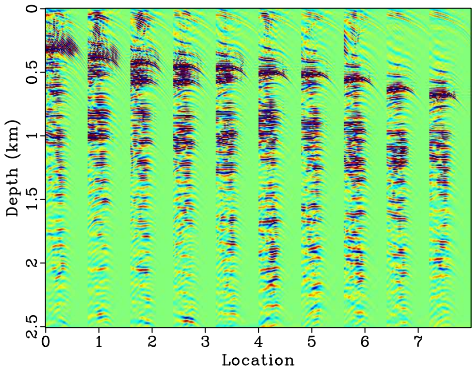

Figure 6: Angle-domain CIGs using the inverted velocity model.

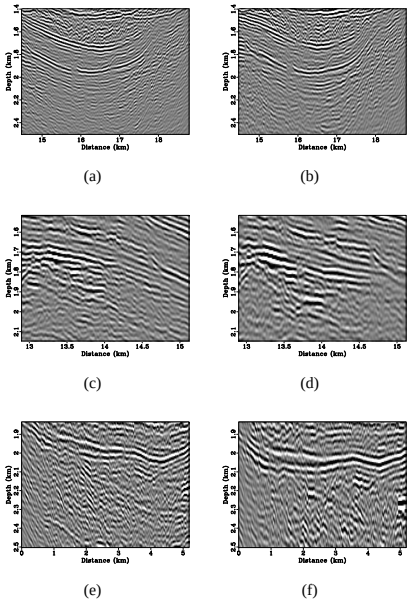

Figure 7: (a), (c) and (e) are the zoomed views from Figure 3. (b), (d) and (f) are the zoomed views from Figure 4.

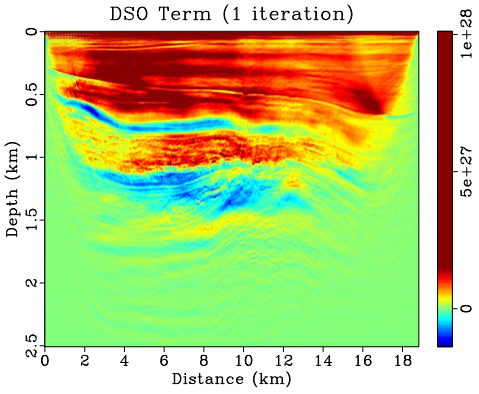

Figure 8: DSO term in the gradient of image-domain FWI.

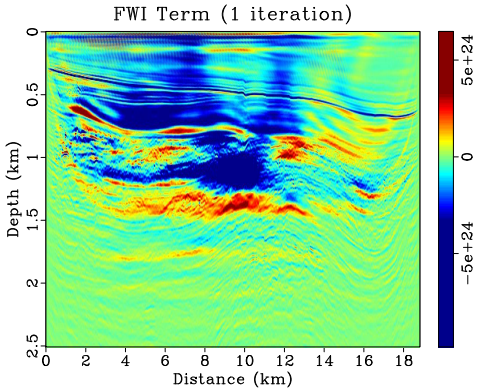

Figure 9: The FWI term in the gradient of image-domain FWI.

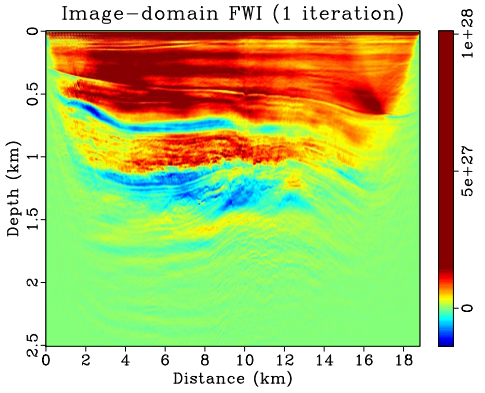

Figure 10: The sum of the DOS and FWI terms which is the total gradient of image-domain FWI

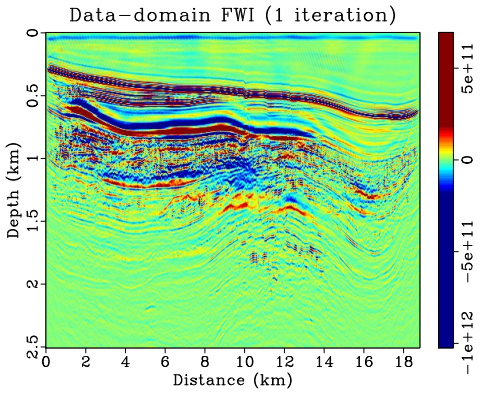

Figure 11: The gradient of conventional FWI.

DOI http://dx.doi.org/10.1190/segam2014-1441.1

http://dx.doi.org/10.1190/segam2014-1441.1

EDITED REFERENCES

Note: This reference list is a copy-edited version of the reference list submitted by the author. Reference lists for the 2014 SEG Technical Program Expanded Abstracts have been copy edited so that references provided with the online metadata for each paper will achieve a high degree of linking to cited sources that appear on the Web.

REFERENCES

Symes, W., and M. Kern, 1994, Inversion of reflection seismograms by differential semblance analysis: Algorithm structure and synthetic examples: Geophysical Prospecting, **42**, no. 6, 565–614, http://dx.doi.org/10.1111/j.1365-2478.1994.tb00231.x.

Yang, T., J. Shragge, and P. Sava, 2013, Illumination compensation for image-domain wavefield tomography: Geophysics, **78**, no. 5, U65–U76, http://dx.doi.org/10.1190/geo2012-0278.1.

Zhang, S., and G. Schuster, 2013, Image-domain full waveform inversion: 83rd Annual International Meeting, SEG, Expanded Abstracts, 861–865.